Magnetic and transport properties of single-grain R-Mg-Zn icosahedral quasicrystals [R=Y, ($Y_{1-x}Gd_x$), ($Y_{1-x}Tb_x$), Tb, Dy, Ho, and Er]

I. R. Fisher, K. O. Cheon, A. F. Panchula,* and P. C. Canfield
Ames Laboratory and Department of Physics and Astronomy, Iowa State University, Ames, Iowa 50011

M. Chernikov and H. R. Ott
Laboratorium für Festkörperphysick, ETH-Hönggerberg, CH-8093 Zurich, Switzerland

K. Dennis
Ames Laboratory, Iowa State University, Ames, Iowa 50011
(Received 2 June 1998)

We report measurements of the dc magnetization, the low-field ac magnetic susceptibility, and the electrical resistivity of large (up to 0.5 cm^3) single-grain samples of icosahedral R-Mg-Zn (R=Y, Tb, Dy, Ho, and Er). The dc magnetization and ac magnetic susceptibility data both indicate that icosahedral Tb-Mg-Zn and Dy-Mg-Zn undergo a transition to a spin-glass state at T_f=5.8 and 3.6 K, respectively, while low-temperature ac susceptibility measurements show that T_f=1.95 and 1.3 K for Ho-Mg-Zn and Er-Mg-Zn, respectively. For the series of solid solutions ($Y_{1-x}Tb_x$)-Mg-Zn, the freezing temperature T_f varies approximately as $x^{2/3}$. The ($Y_{1-x}Gd_x$)-Mg-Zn solid solutions have lower T_f values than ($Y_{1-x}Tb_x$)-Mg-Zn for the same magnetic rare-earth concentrations (x), indicating that local moment anisotropy caused by crystalline electric-field effects plays a significant role in increasing T_f. On the other hand, angular-dependent studies show that the dc magnetization for $T>T_f$ is isotropic within the experimental uncertainty. The electrical resistivity $\rho(T)$ of the single-grain samples is only weakly temperature dependent, with a small, negative $d\rho/dT$. Absolute values of the resistivity fall in the range between 150 and 200 $\mu\Omega$ cm, which is distinctly lower than the values previously reported for other thermodynamically stable icosahedral quasicrystals. [S0163-1829(99)05801-4]

I. INTRODUCTION

The R-Mg-Zn (R=Y, Tb, Dy, Ho, and Er) thermodynamically stable icosahedral quasicrystals are of tremendous interest because they allow the study of the effects of quasiperiodicity on the magnetism of localized $4f$ moments. Previous investigations of the magnetic, thermal, and transport properties of icosahedral R-Mg-Zn have so far been carried out on polygrain samples.[1,2] Recent advances in the growth of large single-grain R-Mg-Zn quasicrystals[3] with volumes of up to 0.5 cm^3 have allowed the investigation of possible anisotropies in the physical properties of these materials. The use of single-grain samples also eliminates the effects of second phases and grain boundaries upon the measured physical properties.

A number of authors have measured the magnetic properties of polygrain R-Mg-Zn quasicrystals. Using polygrain samples, Hattori *et al.*[1] and Charrier and Schmitt[2] showed that the dc magnetic susceptibilities of $R_8Mg_{42}Zn_{50}$ (R=Gd, Tb, Dy, Ho, Er) exhibit a Curie-Weiss–type behavior over a wide temperature range, with a negative Weiss temperature θ [where $\chi=C/(T-\theta)$], indicating antiferromagnetic exchange interactions between the rare-earth moments. At lower temperatures, both ac and dc susceptibility measurements of polygrain $R_8Mg_{42}Zn_{50}$ exhibit a classic spin-glass transition with freezing temperatures T_f below 10 K.[1,2] A later paper by Charrier, Ouladdiaf and Schmitt,[4] however, presented evidence from powder neutron-diffraction measurements that there is a transition to a state with a quasiperiodic type of antiferromagnetic long-range order at $T_N>T_f$ for R=Tb, Ho, Dy, and Er. The intensity of the sharp peaks in the diffraction pattern corresponding to the antiferromagnetic ordering is small and is accompanied by significant diffuse magnetic scattering.[4] Recently, Islam *et al.*[5] showed from neutron-scattering results that there is no such evidence for antiferromagnetic ordering in powders made from large single-grain samples. However, using rapidly cooled polygrain samples the authors[5] were nevertheless able to reproduce some of the additional magnetic diffraction peaks reported in Ref. 4. It remains a contested point whether there exists long-range magnetic order in the R-Mg-Zn family of icosahedral quasicrystals, or whether the additional diffraction peaks seen for polygrain samples are in fact due to the magnetic ordering of small amounts of a rare-earth containing second phase (see Appendix). Another possible explanation is that there is a range of compositions of formation of the thermodynamically stable R-Mg-Zn quasicrystals, and that the magnetic ordering is particularly sensitive to the rare-earth concentration.[5] In either case, the fact remains that any long-range magnetic ordering in R-Mg-Zn quasicrystals is, at best, far from robust.

In this paper, we present the results of detailed magnetic measurements of high-quality, *single-grain*, R-Mg-Zn quasicrystals (R=Y, Tb, Dy, Ho, and Er). The spin freezing transition is investigated in detail by a variety of techniques, including measurements of higher harmonics of the low-frequency ac susceptibility. We also establish, via angular-dependent studies, that for $T>T_f$ the magnetization is iso-

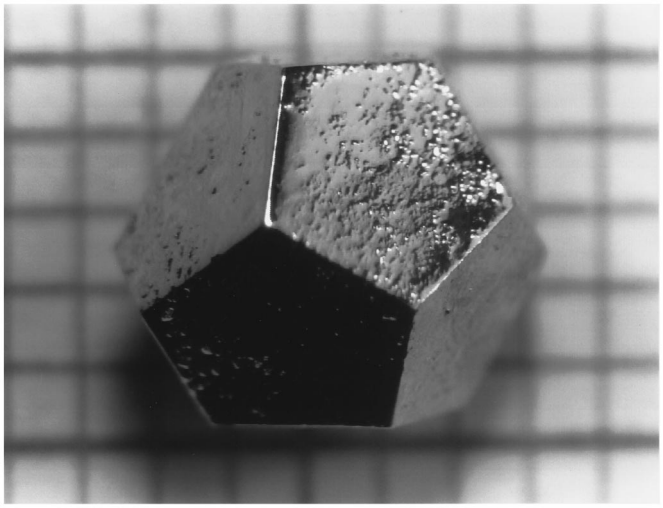

FIG. 1. Photograph of a single-grain icosahedral Ho-Mg-Zn quasicrystal grown from the ternary melt. Shown over a mm scale, the edges are 2.2 mm long. Note the clearly defined pentagonal facets, and the dodecahedral morphology.

tropic within experimental resolution. In addition, we study two pseudoternary compounds, $(Y_{1-x}Tb_x)$-Mg-Zn and $(Y_{1-x}Gd_x)$-Mg-Zn, and examine the effects of rare-earth concentration and CEF (crystalline electric field) splitting on T_f. Results of electrical resistivity measurements are also presented. For comparison, the magnetic properties of a closely related R-Mg-Zn crystalline phase are presented as an appendix.

II. SAMPLE PREPARATION

Single-grain samples of R-Mg-Zn quasicrystals (R=Y, Tb, Dy, Ho, Er) were grown from the ternary melt following the technique described in Ref. 3 In brief, this method involves the slow cooling of a ternary melt intersecting the primary solidification surface of the quasicrystalline phase, as identified for Y-Mg-Zn by Langsdorf, Ritter and Assmus.[6] Large, single-grain samples can be grown by this technique, with volumes of up to 0.5 cm^3. Following the growth, a brief dip in a dilute solution of nitric acid in methanol can be used to remove any small amounts of undecanted flux or oxide slag that wet the surface. A photograph of a typical Ho-Mg-Zn quasicrystal is shown in Fig. 1, over a mm scale. As can be seen from Fig. 1, the quasicrystals grown by this technique have a dodecahedral growth habit, with clearly defined pentagonal facets. It should be noted that the R-Mg-Zn quasicrystal samples grown by this technique are remarkably large and exceptionally well ordered.[3]

Following the same growth procedure, samples with various amounts of substitution of Tb and Gd for Y were also prepared, enabling investigation of magnetic and transport properties as a function of the rare-earth concentration. In particular, the substitutions studied were $(Y_{1-x}Tb_x)$-Mg-Zn with x=0.075, 0.15, 0.33, 0.50, 0.63, 0.75, and 0.88 and $(Y_{1-x}Gd_x)$-Mg-Zn with x=0.075, 0.15, 0.50, and 0.60. The Gd substitutions are of additional interest because the pure Gd-Mg-Zn quasicrystalline phase cannot be grown by this technique.[3] In fact, x=0.60 is the largest amount of Gd substitution in Y-Mg-Zn that we have been able to successfully incorporate as a single-phase quasicrystal. It remains a possibility that the pure Gd-Mg-Zn phase is metastable, and can only be prepared by rapid solidification techniques[1] (in contrast to the slow cooling rate growth technique we employ).

Powder x-ray-diffraction patterns of crushed single grains have narrow peaks, indicating a high degree of structural order, and all peaks can be indexed to the face-centered icosahedral (FCI) quasicrystalline phase (second phases, if present at all, are below a 2–5% level).[3] High-resolution transmission electron microscopy (TEM) reveals very sharp diffraction spots in selected area diffraction patterns (SADP's), with little or no evidence of phason strain seen in lattice images near Scherzer defocus.[3] Electron microprobe analysis of Tb-Mg-Zn quasicrystalline samples indicate a composition of approximately $Tb_9Mg_{34}Zn_{57}$,[3] similar to that estimated by other groups [$R_8Mg_{42}Zn_{50}$ (Refs. 1 and 7) and $R_9Mg_{30}Zn_{61}$ (Ref. 6)].

Clean, well-formed single grains were selected for magnetization measurements. Bars for electrical transport measurements were cut from single grains using a wire saw. Typical bar lengths were 2–3 mm with a width (and thickness) of 0.5 mm. For icosahedral symmetry, the electrical resistivity tensor has only one independent component, and hence the orientation of the cut bars is not expected to effect the results of the resistivity measurements.

III. EXPERIMENTAL METHODS

Both ac and dc magnetization were measured using commercial Quantum Design superconducting quantum interference device (SQUID) magnetometers, in a variety of applied magnetic fields (up to 55 000 Oe) and temperatures (from 1.8 to 350 K). The dc magnetization was investigated for a range of applied fields, and for both zero-field-cooled (zfc) and field-cooled (fc) histories. An applied field of 1000 Oe was used to measure the temperature-dependent dc susceptibility for $T > T_f$. The ac magnetization was measured between 1.8 and 20 K in a steady applied field H_{dc}=100 Oe, with an ac field H_{ac}=2 Oe superimposed, and for a range of frequencies from 1 to 1000 Hz. The angular dependence of the dc magnetization was measured, using a rotating sample platform, with an angular resolution of $\pm 0.1°$. All temperature-dependent magnetization measurements were made for increasing temperatures, and warming through the boiling point of liquid helium was treated carefully. After collecting data from 1.8 to 4.4 K, the cryostat design required that the temperature be cycled from 4.4 K to a higher temperature (usually 30 K) before zero-field-coding or field-cooling (depending on the experiment) down to 4.6 K. Relaxation effects for temperatures below the spin freezing transition (see later sections) can lead to an apparent discontinuity in the zfc magnetization of Tb-Mg-Zn (for which T_f=5.8 K) at 4.4 K as a consequence of this technique.

The low-frequency and low-field ac magnetic susceptibility was measured by a conventional mutual inductance technique in the temperature range between 0.4 and 4 K. Measurements were made at frequencies 116 and 420 Hz and with an excitation magnetic-field amplitude of 0.1 Oe. A low-noise signal transformer was used to match the impedance of the pickup coil with that of the lock-in amplifier. The in-phase component χ' and the out-of-phase component χ''

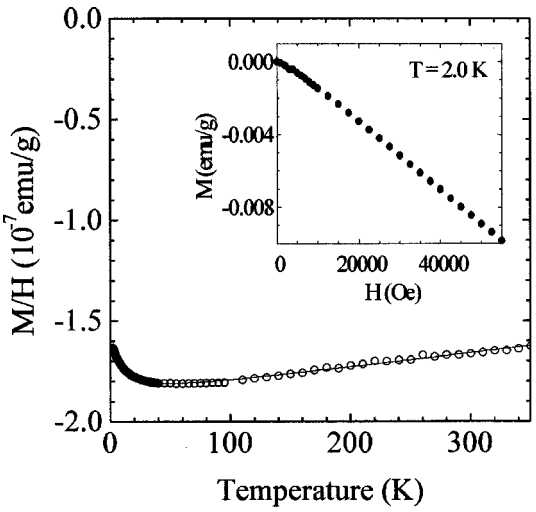

FIG. 2. The dc magnetic susceptibility of icosahedral Y-Mg-Zn, measured in 20 000 Oe. A solid line shows fit using Eq. (1) as explained in the text. Inset shows magnetization as a function of applied field at 2.0 K.

were measured with a two-phase lock-in amplifier. The third-order magnetic susceptibility χ_3 was measured by monitoring the amplitude and the phase of the ac magnetization at the third harmonic $3f$ of the excitation frequency f using the phase-sensitive detector, which was set to detect the response at $3f$.[8]

The electrical resistivity was measured between 1.8 and 300 K using a standard four-probe technique, with an ac bridge operating at 16 Hz, and using current densities of between 0.1 and 1 A/cm^2. Electrical contact was made to the samples using Epo-tek H20E silver epoxy, with typical contact resistances of 1–2 Ω. Due to the uncertainty of the bar dimensions and the contact separation, there is an approximate uncertainty of ±10% in absolute values of the resistivity obtained for individual samples. To give a greater confidence in the absolute value of the resistivity obtained, three different samples of the Y-Mg-Zn quasicrystalline phase have been measured.

IV. RESULTS AND ANALYSIS

A. dc magnetization

The dc magnetic susceptibility of icosahedral Y-Mg-Zn measured in an applied field of 20 000 Oe between 2 and 350 K is shown in Fig. 2. Between 20 and 350 K, the $\chi(T)$ data can be well fit to

$$\chi=\chi_0+\frac{C}{T}+BT \tag{1}$$

with the following values of the fit parameters: $\chi_0=(-1.88\pm0.01)\times10^{-7}$ emu/g, $C=(1.79\pm0.05)\times10^{-7}$ emu K/g, and $B=(7.3\pm0.1)\times10^{-11}$ emu/g K. In Fig. 2, the fit is shown as a solid line. The Curie term C/T is probably due to magnetic rare-earth impurities on the Y sites, and the value of the Curie constant C is consistent with the purity levels of the starting materials (99.99%). The temperature-independent susceptibility χ_0 comprises contributions from itinerant electrons and core states. The origin of the small, positive linear term BT is at present unknown. The field dependence of the magnetization M at 2.0 K is shown in the inset to Fig. 2. The low-field nonlinearity of the $M(H)$ curve is likely due to the Brillouin function saturation of the magnetic impurities (small in value), leaving a linear diamagnetic response due to Y-Mg-Zn.

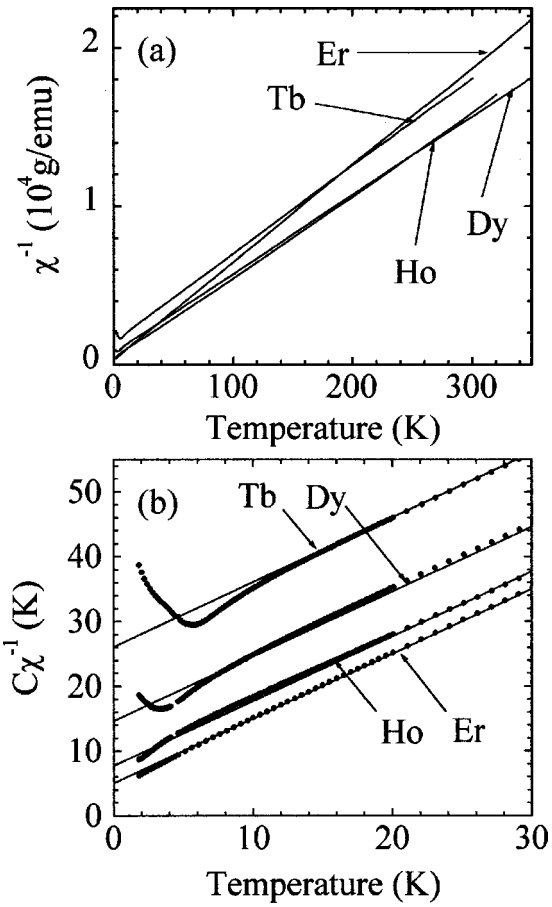

FIG. 3. (a) The inverse dc magnetic susceptibility of quasicrystalline R-Mg-Zn (R=Tb, Dy, Ho, Er), measured in 1000 Oe, plotted as a function of temperature T. (b) shows the same data normalized by the values of the Curie constant C obtained as explained in the text. Lines show extrapolation of high-temperature ($T>50$ K) fits using the Curie-Weiss law.

The dc magnetic susceptibility (where we define $\chi=M/H$ for these low-field measurements) of the magnetic rare-earth containing R-Mg-Zn quasicrystalline samples (R=Tb, Dy, Ho, Er), measured in an applied field of 1000 Oe, is shown in Fig. 3(a) as the plot of χ^{-1} vs T. As can be seen, above 15 K data for all four compounds follow a good Curie-Weiss–type temperature dependence [where $\chi=C/(T-\theta)$ and θ is the Weiss temperature]. For each compound, the Curie constant (C) may be obtained and compared to the calculated effective moment $p_{\rm eff}$ per rare earth, allowing an estimation of the relative molecular mass (RMM) per rare-earth ion. From the data shown in Fig. 3 we obtain the RMM values given in Table I. The given uncertainty of ±1 g/mol R corresponds to standard deviations in the linear fits to the data, and does not include experimental uncertainties that are better reflected in the spread of ±30 g/mol R in the RMM values. These uncertainties might arise from the presence of small amounts of impurities on the surface of the samples

TABLE I. Summary of the parameters obtained from the dc and ac susceptibility data for R-Mg-Zn (R = Tb, Dy, Ho, and Er).

System	C (g/emu K)	RMM (g/mol R)	θ (K)	T_f (K)
Tb-Mg-Zn	0.0180±0.0001	655±1	−26.3±0.4	5.80±0.05[a]
Dy-Mg-Zn	0.0201±0.0001	705±1	−14.8±0.4	3.60±0.05[a]
Ho-Mg-Zn	0.0195±0.0001	720±1	−7.8±0.4	1.95±0.05[b]
Er-Mg-Zn	0.0163±0.0001	704±1	−5.1±0.4	1.30±0.05[b]

[a]Position of the maximum in zfc $\chi_{dc}(T)$.
[b]Position of the maximum in $\chi'_{ac}(T)$.

(undecanted flux from the growth). Our data indicate that the RMM=690±30 g/mol R for the R-Mg-Zn series. The RMM values are consistent with the results of the electron microprobe analysis, that showed that Tb-Mg-Zn quasicrystalline samples gave the stoichiometry $R_{8.7}Mg_{34.6}Zn_{56.8}$, which corresponds to an RMM of 682 g/mol Tb.[3]

In Fig. 3(b), we show the magnetic susceptibility data plotted as C/χ vs T, where C is the fit value of the Curie constant determined as described above. This normalization renders the high-temperature $\chi^{-1}(T)$ data with equal slopes (value 1), and more clearly reveals the Weiss temperatures. In Fig. 3(b), $-\theta$ is given by the intercept with the y axis of the extrapolation of the high-temperature Curie-Weiss law fit (shown by solid lines). The Weiss temperatures for each of the four magnetic compounds are given in Table I. All four θ values are negative, indicating antiferromagnetic exchange interactions between magnetic moments. The θ values approximately scale with the de Gennes factor $(g-1)^2J(J+1)$ of the magnetic rare-earth elements (see later discussion and Fig. 15), and are in agreement with values previously obtained for polygrain samples.[2] The absence of any clearly visible evidence for long-range magnetic ordering at comparable temperatures to $-\theta$ in these single-grain samples[5] is consistent with geometric frustration of the magnetic moments. This might arise from the multiplicity of R-R distances (due to the quasicrystalline environment) leading to frustration due to the distance-dependent Ruderman-Kittel-Kasuya-Yosida (RKKY) interaction. The low carrier concentration as compared to conventional metals (characteristic of many quasicrystalline materials) might mean that the local environment around each R ion plays a significant part in the origin of the magnetic frustration, in addition to the R-R interactions. This point is returned to later on, when considering the magnetization of $(Y_{1-x}Tb_x)$-Mg-Zn and $(Y_{1-x}Gd_x)$-Mg-Zn. The low-temperature upturns in the inverse susceptibility data shown in Fig. 3 are associated with a spin-glass freezing transition (a consequence of the massive frustration) and are discussed in detail below.

The inverse susceptibility data in Fig. 3(b) show distinct deviations from the Curie-Weiss law a few Kelvin above the spin freezing transition [evident from a downturn from the extrapolated high-temperature linear fit, shown by straight lines in Fig. 3(b)]. Canonical spin glasses with antiferromagnetic interactions [for example, $Au_{1-x}Fe_x$ with $x<3$ at. % Fe (Ref. 9) and $Pt_{1-x}Mn_x$ alloys with $x<10$ at. % Mn (Ref. 10)] show similar deviations for $T>T_f$, which can be associated with antiferromagnetic clusters forming above T_f. Similar behavior has also been observed for icosahedral Al-Pd-Mn quasicrystals with a Mn concentration of 9 at. %.[11] The preformation of magnetic clusters might make it tempting to classify the R-Mg-Zn quasicrystals as superparamagnets. However, the effect is actually quite small, and a more detailed investigation of the spin freezing via magnetic measurements (see below) indicates that the classification as a spin glass is indeed more appropriate. As a final comment on the low-temperature deviation from the Curie-Weiss law, we note that a similar temperature dependence is observed for Gd dilutions in Y-Mg-Zn (see Sec. IV F), for which the crystal electric field (CEF) has negligible effect, which is empirical evidence that the deviations cannot be due to CEF effects.

B. Angular dependence of the dc magnetization above T_f

The growth of macroscopic single-grain samples has allowed investigation of the angular dependence of the magnetization of R-Mg-Zn quasicrystals. The possibility of in-

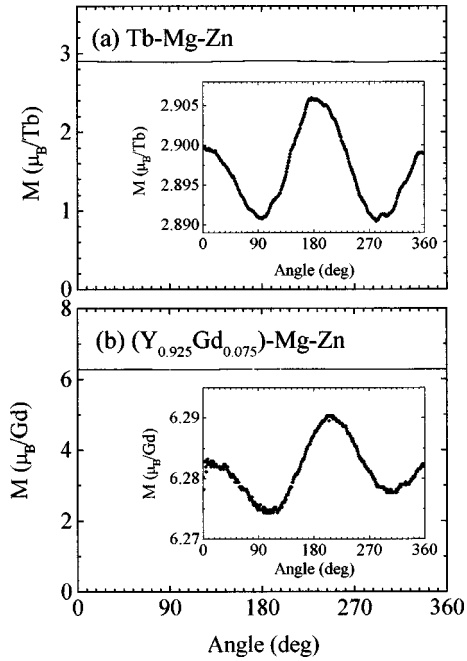

FIG. 4. The angular dependence of the magnetization of (a) Tb-Mg-Zn and (b) $(Y_{0.925}Gd_{0.075})$-Mg-Zn quasicrystalline samples for temperatures greater than the spin freezing transition. Insets to each figure show the same data on expanded scales. Measurements were made in applied fields of 55 000 Oe, and at temperatures of 10.0 and 2.0 K for each compound, respectively.

vestigating rare-earth ions in crystallographically forbidden-point symmetries (which are allowed in quasicrystals) is particularly enticing. Using a rotating sample platform, the dc magnetization of several members of the *R*-Mg-Zn family (and also several dilutions of magnetic rare earths in Y-Mg-Zn) has been investigated as a function of angle ϕ, for a given plane of rotation chosen to include directions of two-fold, threefold, and fivefold rotational symmetry. In each case, measurements were made for temperatures greater than T_f.

Representative data for Tb-Mg-Zn and $(Y_{0.925}Gd_{0.075})$-Mg-Zn (measured at $T=10.0$ and 2.0 K, respectively) are shown in Fig. 4. In each case, the $M(\phi)$ data are essentially isotropic, with only a small and approximately sinusoidal angular dependence to the magnetization, with a period of 180° and an amplitude of approximately 0.1–0.2% of the average magnetization [as indicated by expanded insets in Figs. 4(a) and 4(b)]. The fact that the same behavior is seen for the $(Y_{0.925}Gd_{0.075})$-Mg-Zn sample [Fig. 4(b)] as for Tb-Mg-Zn [Fig. 4(a)] indicates that the small sinusoidal angular dependence is not due to crystal electric fields, which do not affect Gd moments (for which the orbital angular momentum of the Hund's rule ground-state *J* multiplet *L* is zero). The observed sinusoidal angular dependence is actually associated with details of our measurement technique, and is due to slight asymmetries of sample position on the rotating probe head (the measured data have not been corrected for this asymmetry to convince the reader that even the raw data show these materials to be remarkably isotropic). Small deviations from the sinusoidal angular dependence are probably due to changes in the geometric demagnetization factor as the samples rotate in the applied field (the samples were not exactly spherical, but were in general faceted and slightly oblate), and these deviations are entirely consistent with our $M(H)$ data and sample geometries. In short, for $T>T_f$ the magnetization of the *R*-Mg-Zn quasicrystals is isotropic within experimental uncertainty. The absence of any experimentally significant angular dependence to the magnetization is likely the result of there being many different rare-earth sites in the quasicrystals, all of which average to give an isotropic response. Controlling the occupancy of different rare-earth sites, for example, in dilution studies such as $Y_{1-x}Tb_x$-Mg-Zn, may be the key to investigating the magnetic anisotropy of individual rare-earth sites, and we note that work is currently in progress to achieve this. Finally, the experimentally observed isotropic bulk magnetization of icosahedral *R*-Mg-Zn implies that sample orientation is unimportant for all magnetic measurements made for $T>T_f$.

C. dc magnetization below T_f

In Fig. 5 we show the dc susceptibility M/H as a function of temperature for icosahedral Tb-Mg-Zn and Dy-Mg-Zn, measured in an applied field of 25 Oe. Both data sets reveal textbook[12] examples of spin-glass-type freezing transitions that are significantly sharper than data previously reported for rapidly cooled polygrain *R*-Mg-Zn material.[1,2] The freezing temperatures T_f, defined here as the maximum in the zfc dc magnetization, have values of $T_f=5.8$ and 3.6 K for Tb-Mg-Zn and Dy-Mg-Zn, respectively, and have values below

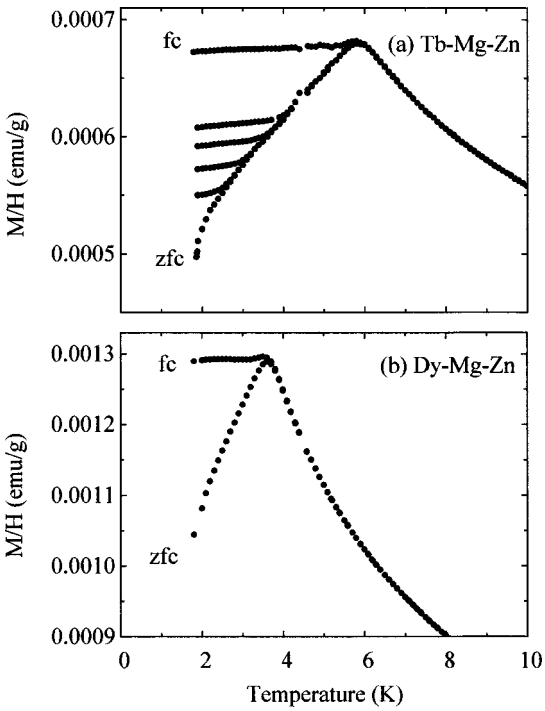

FIG. 5. The low-temperature dc magnetization of (a) Tb-Mg-Zn and (b) Dy-Mg-Zn in an applied field of 25 Oe, for both zero-field-cooled (zfc) and field-cooled (fc) histories. Also shown for Tb-Mg-Zn are fc data from temperatures of 2.5, 3.0, 3.5, and 4.0 K following an initial zfc (as described in main text).

2.0 K for Ho-Mg-Zn and Er-Mg-Zn (see Sec. IV D and Fig. 10). Above T_f both zfc and fc data are identical. Below T_f the zfc magnetization decreases with decreasing temperature, while the fc data remain almost temperature independent. Additional data for Tb-Mg-Zn [Fig. 5(a)] show the effect of field cooling from various temperatures $T'<T_f$ (following an initial zero-field cooling to 1.8 K and warming in 25 Oe from 1.8 K to T'). The magnetization data taken while warming after field cooling from T' are almost temperature independent up to T', after which they fall on the original zfc manifold, and are further evidence of a spin-glass state below T_f.

Below T_f, the zfc magnetization is strongly affected by relaxation processes, empirically governed by a stretched-exponential time relationship (see Sec. IV E). Such relaxation effects make quantitative measurements of $M(T,t)$ for $T<T_f$ very complex. In particular, this relaxation leads to the small step seen at 4.2 K in Fig. 5(a) because the cryostat used for these measurements requires the cycling of temperatures past the boiling point of liquid helium to above T_f followed by a subsequent zero-field cooling to just above 4.2 K (as described in Sec. III).

The dc magnetization of Tb-Mg-Zn was investigated in a range of applied fields from 10 to 55 000 Oe, and results are presented in Fig. 6 (data for applied fields of 10 and 25 Oe are virtually identical with those for $H=100$ Oe, and are therefore not included). Data for $H=100$, 1000, and 10 000 Oe are shown separately in Fig. 6(a) to more clearly illustrate the effect of the applied field on the spin freezing transition, while Fig. 6(b) shows similar data for all of the fields measured. Note that the breaks in the data at 4.2 K are again due to the measurement technique, as described above.

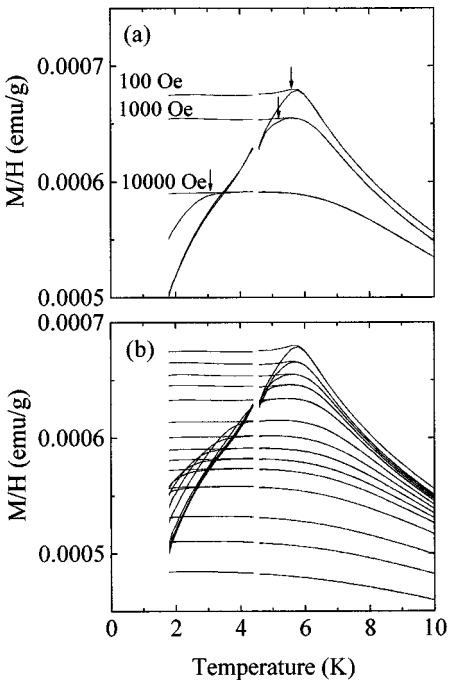

FIG. 6. The low-temperature zfc and fc dc magnetization of Tb-Mg-Zn for various applied magnetic fields. For clarity, panel (a) shows data for $H=100$, 1000, and 10 000 Oe, while panel (b) shows similar data for all fields measured: $H=100$, 500, 1000, 1500, 2500, 5000, 7500, 10 000, 12 500, 15 000, 20 000, 30 000, 40 000, and 55 000 Oe (increasing field from top to bottom of figure). For applied fields less than 30 000 Oe, the zfc data are lower in value than the fc data for $T<T_{\rm ir}$. Arrows indicate $T_{\rm ir}$ for the data in panel (a), where $T_{\rm ir}$ is the onset-of-irreversibility temperature (as determined by criterion described in main text).

The applied magnetic field has several pronounced effects on the temperature dependence of the magnetization $M(T)$. A sharp peak in the zfc magnetization is observed for the smaller applied fields (10–100 Oe), but significant broadening and flattening of the peak is observed in larger fields. This effect has also been observed for other spin glasses, for example, $Ag_{1-x}Mn_x$,[13] although the flattening of the magnetization $M(T)$ near to T_f in larger applied magnetic fields is more pronounced in our case. In addition, while the smaller applied fields yield a dc susceptibility of Tb-Mg-Zn that deviates from the Curie-Weiss law below approximately 12 K [see Fig. 3(b)], this deviation is suppressed by larger applied fields. In fact, an applied field of 10 000 Oe completely suppresses the downturn in $\chi^{-1}(T)$ for Tb-Mg-Zn seen in Fig. 3(b). This is consistent with the deviation being due to the formation of antiferromagnetic clusters, remembering that applied fields suppress antiferromagnetic correlations. Significantly larger applied fields ($H>20\,000$ Oe) also result in small deviations from the Curie-Weiss law for $T>T_f$, but in this case because of the Brillouin function saturation of the Tb moments [i.e., the larger fields are beyond the low-field linear regime of $M(H)$].

For applied magnetic fields of less than 30 000 Oe, the zfc dc magnetization is lower than the fc dc magnetization below the spin freezing transition (Figs. 5 and 6). However, for intermediate values of the applied field, the temperature $T_{\rm ir}$ at which there is an onset of irreversibility in the magnetization (i.e., the point at which fc and zfc data start to deviate) is no longer at the center of the significantly broadened peak in the magnetization $M(T)$. A criterion of 0.5% deviation of the zfc magnetization from the fc magnetization was chosen to determine the onset-of-irreversibility temperature $T_{\rm ir}$. Arrows in Fig. 6(a) indicate $T_{\rm ir}$ for those data, and the applied magnetic fields H are plotted as a function of $T_{\rm ir}$ in Fig. 7 for all fields measured. The data can be well fitted by

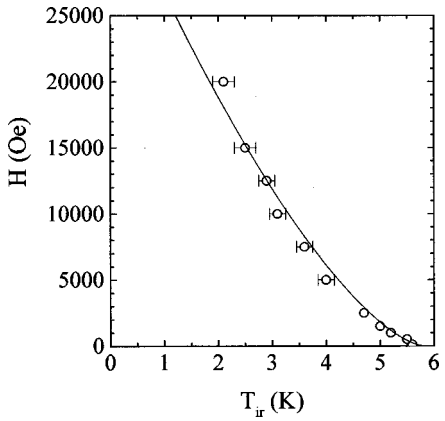

FIG. 7. The field dependence of $T_{\rm ir}$ for Tb-Mg-Zn, as deduced from data shown in Fig. 6. Line shows fit to Eq. (2).

$$H(T_{\rm ir})=\alpha\left(1-\frac{T_{\rm ir}}{T_f}\right)^{3/2}, \tag{2}$$

with $\alpha=(3.5\pm0.1)\times10^4$ Oe, using the peak in the low-field $M(T)$ data to define $T_f=5.8$ K. A fit to our $T_{\rm ir}(H)$ data using Eq. (2) is shown in Fig. 7 as a solid line. This $T_{\rm ir}(H)$ variation (de Almeida–Thouless-like line[14,15]) has previously been reported for various other spin-glass systems.[13,16]

D. ac magnetic susceptibility

The in-phase component χ' and the out-of-phase component χ'' of the ac magnetic susceptibility for icosahedral Tb-Mg-Zn, measured in the temperature range from 1.8 to 15 K and for selected frequencies between 1 and 1000 Hz, are shown in Figs. 8(a) and 8(b), respectively. Both zero-field-cooled and bias-field-cooled data are shown. As also observed for the zfc dc magnetization (Fig. 5), there is a sharp peak in χ' which can be used to define T_f. However, in contrast to the dc magnetization, the susceptibilities (i.e., $\partial M/\partial H$) of both the zfc and fc states are identical for temperatures both above and below the freezing temperature. This is despite the large difference in the actual magnetization [plotted as M/H in Fig. 8(a) for comparison] between zfc and fc states below T_f. At least for this case of $H_{\rm ac}$ (2 Oe)$\ll H_{\rm dc}$ (100 Oe), the spin glass is most likely trapped in a metastable state, and these data therefore imply that all metastable states behave similarly in small perturbative fields $H_{\rm ac}$. The out-of-phase component χ'' is vanishing above T_f, but is nonzero for $T<T_f$, implying dissipation not only at the freezing transition but also for temperatures below it, a common feature of spin glasses.[17] Similar to other spin glasses,[12] the maximum slope in χ'' correlates with the peak in χ'.

The peak in χ' shifts to higher temperatures as the frequency (f) increases, with T_f (defined here as the peak in χ')

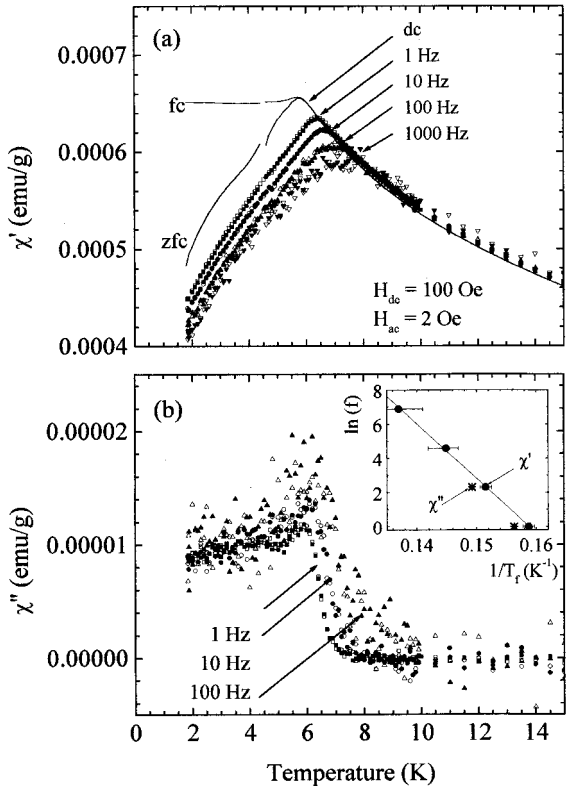

FIG. 8. The zero-field-cooled (solid symbols) and bias-field-cooled (open symbols) ac susceptibility of Tb-Mg-Zn, measured for different applied frequencies from 1 to 1000 Hz (listed in figure). Measurements were made in a steady bias field of 100 Oe with a 2-Oe ac field superimposed. Top panel (a) shows real part χ', and bottom panel (b) shows imaginary part χ''. dc magnetization (also measured in 100 Oe) is shown in top panel, for both zfc and fc cases. Inset to panel (b) shows the natural log of the frequency vs $1/T_f$, where the freezing temperature T_f has been defined as the maximum in χ' (solid circles) and the extrapolation to zero of the sharp rise in χ'' (stars). Line shows best linear fit to T_f data from χ'.

having values of 6.3, 6.6, 6.9, and 7.3 K for measurement frequencies of 1, 10, 100, and 1000 Hz, respectively. [Note that the dc data are not considered as a zero-frequency limit to the ac susceptibility for the following analysis, and are only included in Fig. 8(a) for comparison.] These data allow us to calculate the fractional relative change in the freezing temperature per decade change in frequency, $\Delta T_f/(T_f \Delta \log_{10} f)$, where ΔT_f is the change in T_f for the given change in frequency ($\Delta \log_{10} f = 3$), and we use the average value of $T_f = 6.8$ K for this range of frequencies. Using these values we find that $\Delta T_f/(T_f \Delta \log_{10} f) = 0.049$, a factor of 10 greater than observed for $Cu_{1-x}Mn_x$ but comparable to that of several other canonical spin glasses.[12]

The frequency dependence of T_f can be fitted by an activated behavior, as shown by the plot of $\ln(f)$ vs $1/T_f$ in the inset to Fig. 8(b). However, the fit requires unphysically large parameters, characteristic of other spin glasses.[12] The fit to the data shown in Fig. 8(b) results in a value of the prefactor $f_0 = 10^{22}$ Hz and an activation energy $E_a/k_B = 320$ K, which is considerably greater than the characteristic temperature scale. The parameters obtained from the activation analysis are smaller than those of some canonical spin glasses,[12] but nevertheless remain unphysically large. This was expected, since in the spin-glass state there exist many metastable states that cannot be fitted to a simple exponential Arrhenius law. A better description of the experimental data can be obtained using the Vogel-Fulcher law

$$f = f_0 \exp\left(\frac{-E_a}{k_B(T_f - T_0)}\right), \tag{3}$$

which is an empirical law originally used to describe the viscosity of supercooled liquids.[12,18] This law involves a third fit parameter T_0, which might be considered a measure of the interaction strengths between clusters in the spin glass. From the ac susceptibility data shown in Fig. 8, we obtain the following values: $f_0 = (4 \pm 1) \times 10^7$ Hz, $E_a/k_B = 27 \pm 1$ K, and $T_0 = 4.8 \pm 0.1$ K. As for other spin glasses,[18] $T_0 < E_a/k_B$. While a strict physical interpretation of these parameters is still lacking for spin-glass systems, we note that the values obtained for Tb-Mg-Zn are in general agreement with similar parameters previously reported for other spin glasses.[18]

Based on these results, icosahedral Tb-Mg-Zn can be classified as a spin glass with a moderate strength of the RKKY interaction between magnetic moments, mediated by itinerant electrons. For spin glasses with a strong RKKY interaction $T_f - T_0 \ll T_f$, while for metallic spin glasses with a weak RKKY interaction $T_0 \ll T_f$ (Ref. 18) (as observed for Al-Pd-Mn icosahedral quasicrystals[11]). The observed type of relaxation in Tb-Mg-Zn is compatible with a fairly low value of $T_f/x' = 0.66$ K/at. % (where x' is the Tb concentration in at. %). Typical metallic spin glasses are characterized by much higher values of T_f/x', for example, up to 10 K/at. % for $Au_{1-x'}Fe_{x'}$.[19] Values of T_f/x' that are comparable in magnitude with our Tb-Mg-Zn result have previously been reported for spin glasses with a moderate exchange interaction between magnetic moments, mediated by itinerant electrons. An example is the $Sc_{1-x'}Tb_{x'}$ spin-glass system with $T_f/x' = 1.4$ K/at. %.[20]

Although the cusp in the zfc dc susceptibility and in the real part of the ac susceptibility would be indicative of a spin-glass-type freezing of magnetic moments, it is also possible that it results from a blocking of superparamagnetic clusters.[17] Convincing evidence against this scenario is the observed temperature variation of the third-order magnetic susceptibility χ_3 defined in terms of magnetization M and an applied magnetic field H as

$$M = \chi H + \chi_3 H^3 + O(H^5). \tag{4}$$

The third-order susceptibility χ_3 of Tb-Mg-Zn and Ho-Mg-Zn was investigated in the temperature range between 1.6 and 12 K using a low-frequency ac technique, which probes χ_3 directly. For Tb-Mg-Zn, an ac field amplitude of 300 Oe and a frequency of 7 Hz was used, while for Ho-Mg-Zn values of 50 Oe and 21 Hz, respectively were used. Results, presented in Figs. 9(a) and 9(b), show distinct negative anomalies at 6.9 and 1.9 K for Tb-Mg-Zn and Ho-Mg-Zn, respectively. Using the χ' data shown in Fig. 8, it is possible to estimate a value of $T_f \approx 6.6$ K for Tb-Mg-Zn at the measurement frequency of 7 Hz [shown by an arrow in Fig. 9(a)]. The observation of a sharp, negative anomaly in

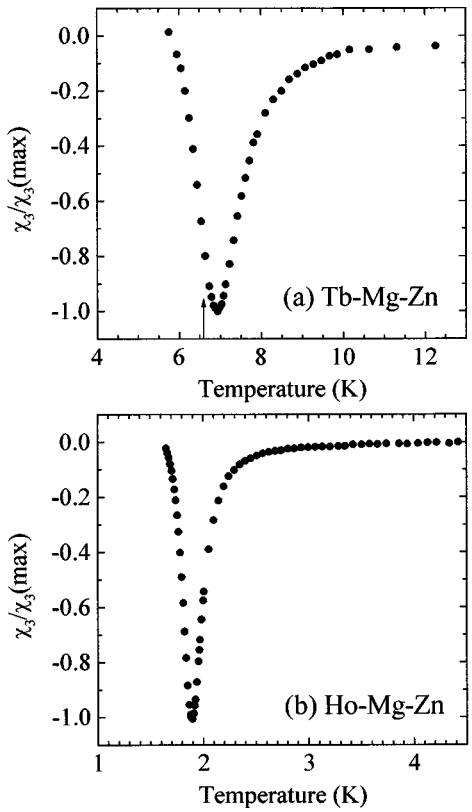

FIG. 9. The third-order ac susceptibility χ_3 of (a) Tb-Mg-Zn (at 7 Hz) and (b) Ho-Mg-Zn (at 21 Hz), normalized by the maximum value χ_3(max). A vertical arrow for Tb-Mg-Zn indicates T_f for a measurement frequency of 7 Hz, estimated from the χ' data shown in Fig. 8.

χ_3 near T_f constitutes strong evidence that the cusp in zfc $\chi_{\rm dc}$ and in χ' corresponds to a spin-glass freezing.[21]

We have also measured the low-field ac magnetic susceptibility for icosahedral Ho-Mg-Zn and Er-Mg-Zn from 0.5 to 4.0 K (dc magnetization measurements were not available

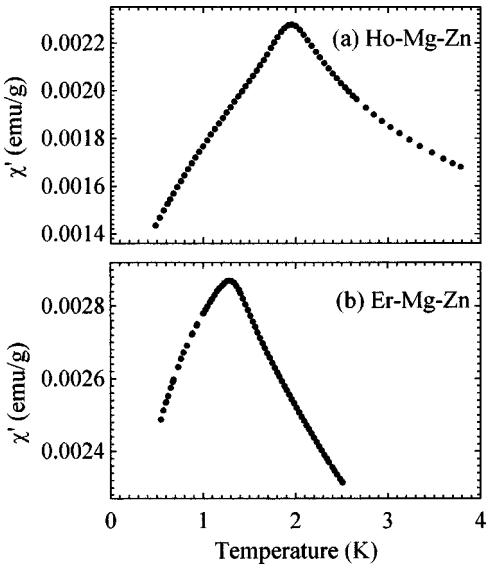

FIG. 10. The real component χ' of the ac susceptibility of (a) Ho-Mg-Zn and (b) Er-Mg-Zn measured at a frequency of 420 and 116 Hz, respectively.

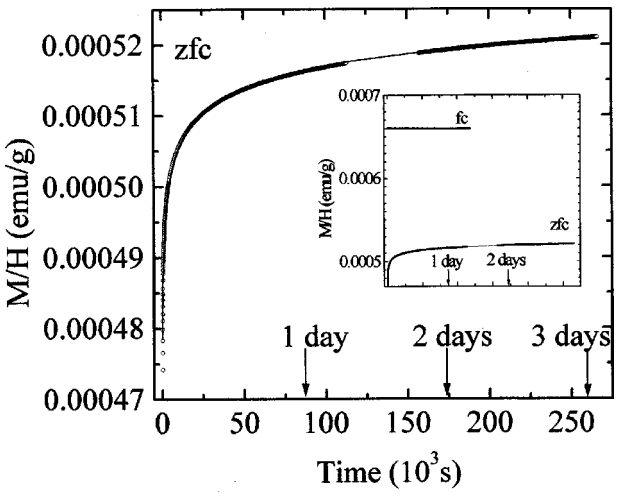

FIG. 11. The time dependence of the zfc magnetization of Tb-Mg-Zn for an applied field of 100 Oe at 2.0 K. Data are shown by open circles, while a solid line shows the best fit to Eq. (5). Inset shows the same zfc data with fc data on the same vertical scale for comparison.

for $T<1.8$ K). While the field and frequency dependence of the $\chi'(T)$ curves was not studied in detail, the $\chi'(T)$ data for selected frequencies are shown in Fig. 10. As can be seen, these two compounds also show a cusp in $\chi'(T)$, at $T_f=1.95\pm0.05$ and 1.30 ± 0.05 K for Ho-Mg-Zn and Er-Mg-Zn, respectively.

E. Relaxation and remanence effects in the dc magnetization

A common feature of spin glasses is that there exist relaxation processes below the freezing temperature that can cause the magnetization to have a time dependence. While it is not in the scope of this particular article to thoroughly investigate these relaxation effects, which is an extensive problem, some initial measurements have been made to demonstrate such properties. In particular, Fig. 11 shows how the zfc dc magnetization of Tb-Mg-Zn at 2.0 K varies with time after applying a field of 100 Oe immediately after stabilizing the temperature at 2.0 K. The inset to Fig. 11 shows equivalent fc data for comparison. Measurements using the SQUID magnetometer take of the order of 1 min, and the applied field also takes approximately 1 min to reach 100 Oe, so consequently any relaxation processes with time constants of order 1 min or less are not observable by this particular technique. However, the zfc data in Fig. 11 clearly demonstrate a relaxation process with effective time constants much longer than the experimental resolution. The data can be well fitted by a stretched exponential

$$\chi(t)=\chi(\infty)-A\ \exp[-(t/\tau)^{\beta}], \tag{5}$$

shown as a solid line in Fig. 11. Here $\chi=M/H$, and the fit parameters have the values $\chi(\infty)=(5.30\pm0.01)\times10^{-4}$ emu/g, $A=(1.0\pm0.1)\times10^{-4}$ emu/g, $\tau=(1.3\pm0.2)\times10^{3}$ s, and $\beta=0.18\pm0.01$. The given uncertainties are statistical in origin, and it should be noted that there is a considerable slackness between the two parameters τ and β. As is evident from this fitting and from inspecting the inset to Fig. 11, the final value that the zfc magnetization is tending

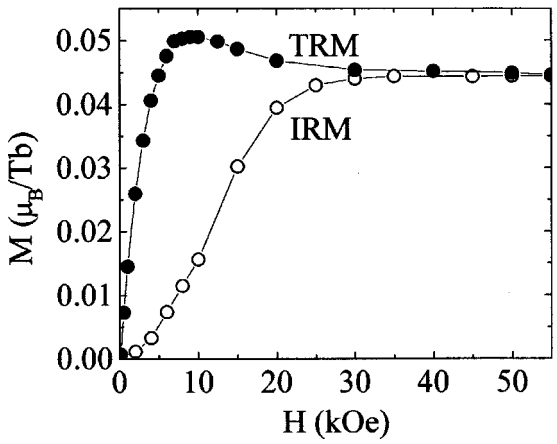

FIG. 12. The isothermal remanent magnetization (IRM) and thermoremanent magnetization (TRM) of Tb-Mg-Zn, measured at 2.0 K. Precise field history and measurement timing as described in the text. Lines are drawn to aid the eye.

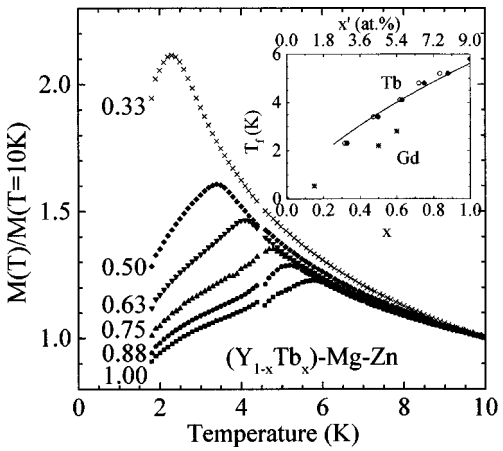

FIG. 13. The zero-field-cooled low-temperature dc magnetization of $(Y_{1-x}Tb_x)$-Mg-Zn quasicrystalline samples (nominal concentrations listed in figure) measured in an applied field of 25 Oe. Magnetization data have been normalized by value at 10 K for clarity. Inset shows freezing temperature T_f as a function of x for nominal Tb concentration (solid circles) and concentration estimated from Curie-Weiss susceptibility (open circles). Inset also shows atomic percentage of magnetic rare earth x'. Solid line shows best fit to the $(Y_{1-x}Tb_x)$-Mg-Zn data using Eq. (6) and nominal concentrations. Stars show T_f values for nominal concentrations of $(Y_{1-x}Gd_x)$-Mg-Zn.

towards $\chi(\infty)=5.3\times10^{-4}$ emu/g is considerably less than the fc value of 6.6×10^{-4} emu/g. However, there is no evidence to suggest that the fc value is relaxing down to the same $\chi(\infty)$ value. The fit value for β (0.18 ± 0.01) is a little lower than the value of 0.33 obtained in more traditional spin glasses [for example, $Cu_{1-x}Mn_x$ and $Ag_{1-x}Mn_x$ (Ref. 22)], and forcing the parameter $\beta=0.33$ results in a poorer fit to our data. The nonunitary value of parameter β indicates that there are several relaxation processes at play, and it is possible that the fit parameter $\chi(\infty)$ may differ from the actual value that the zfc dc magnetization will have after an infinitely long duration. These data may indicate that for the *R*-Mg-Zn spin glasses, the potential barriers between the closely spaced energy levels of the system are particularly high.

In addition to the above, a brief survey of the isothermal remanent magnetization (IRM) and the thermoremanent magnetization (TRM) was made for a single-grain Tb-Mg-Zn sample. The IRM was measured by zero-field cooling the sample, immediately applying a field *H*, and then immediately removing that field and measuring the remanent magnetization after a typical time delay of order 1 min. The TRM was measured by field cooling the sample in field *H*, immediately removing the field, and measuring the remanent magnetization in the same way as for the IRM. In light of the above discussion, relaxation effects may be significant in affecting the measured magnetization values. The typical measurement timescale (approximately 1 min) is significantly shorter than the observed stretched exponential relaxation, but faster relaxation processes cannot be ruled out. The IRM and TRM data for measurements made at 2.0 K are shown in Fig. 12. Both data sets appear to reach a common saturation value of 0.045μB/Tb for applied fields greater than approximately 40 000 Oe. The general form of the IRM and TRM data (Fig. 12) are typical for spin-glass systems.[12]

F. Magnetic properties of Tb- and Gd-substituted Y-Mg-Zn

As mentioned previously, single-grain *R*-Mg-Zn quasicrystal samples were also prepared with various amounts of substitution of Tb and Gd for Y. These dilutions have enabled the investigation of the magnetic and transport properties as a function of the magnetic rare-earth concentration. For all materials, the dc magnetic susceptibility in the temperature range between 50 and 350 K is consistent with the nominal magnetic rare-earth concentrations *x*, assuming the same mass per rare earth as for the pure material. We note that there are probably several classes of sites of different point symmetries in the quasicrystal structure that can be occupied by the rare-earth ions. At the moment, it is not possible to tell whether the rare-earth substitutions occur uniformly for all sites, or whether particular sites are favored.

Figure 13 shows zfc dc magnetization data for the more Tb-concentrated $(x\geqslant0.33)$ $(Y_{1-x}Tb_x)$-Mg-Zn samples listed above (Sec. III). The data, taken in an applied field of 25 Oe, have been normalized, for clarity, by the magnetization value at 10 K. Note that breaks in the data at 4.2 K are again due to the details of the cryostat operation, as described in Sec. III. As can be seen in Fig. 13, the spin-glass freezing temperature T_f (defined here as the maximum value in the zfc dc magnetization) decreases as the Tb concentration (x) decreases. This trend is illustrated in the inset to Fig. 13, showing T_f as a function of x, where values are shown for both nominal x concentration, and x concentration estimated from the high-temperature Curie-Weiss susceptibility (assuming the same mass per rare earth as for the pure material). In the inset to Fig. 13, the magnetic rare-earth concentration is also expressed as a fraction x' of the total number of atoms. The $T_f(x)$ data can be well described by

$$T_f=ax^{2/3}, \tag{6}$$

consistent with the T_f vs x variation previously reported for other spin-glass systems with similar ranges of x'.[12] The fit parameter $a=5.6\pm0.1$ K is consistent with $T_f=5.8$ K for pure Tb-Mg-Zn. The limited data set make it difficult to rule

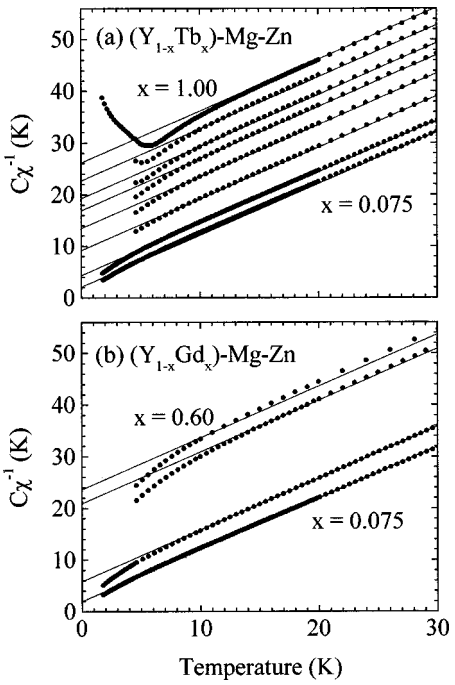

FIG. 14. (a) The inverse dc magnetic susceptibility of the $(Y_{1-x}Tb_x)$-Mg-Zn series (x values given in the text), measured in an applied field of 1000 Oe. Values have been normalized by the high-temperature Curie constant C for each concentration, as described in main text. Lines show extrapolation of high-T Curie-Weiss fit, indicating the Weiss temperatures. Lower panel (b) shows similar data for the $(Y_{1-x}Gd_x)$-Mg-Zn series.

out a linear dependence for $x>0.7$ ($x'>6$ at. %) which one might expect for the concentration regime for which cluster glass behavior can become significant ($x'>10$ at. %).[12] Given the underlying lack of periodicity in the quasicrystal environment, it may be that the $x^{2/3}$ power law would persist to even larger values of x' than for conventional crystalline spin-glass systems, although approximately 9 at. % is the maximum Tb concentration available with this system (i.e., $Tb_9Mg_{34}Zn_{57}$).[3]

In addition to the Tb dilutions discussed above, substitutions of Gd for Y were also prepared for $(Y_{1-x}Gd_x)$-Mg-Zn with several concentrations x in the range between 0.075 and 0.6. The pure Gd-Mg-Zn FCI quasicrystal phase ($x=1.0$) cannot be prepared via the self-flux methods used for the growth of the single-grain R-Mg-Zn samples described in this paper.[3] The Gd substitutions described above are therefore significant in allowing the study of the Gd moment in the quasicrystal environment, where pure Gd-Mg-Zn samples are not available.

As already described (Sec. IV B), measurements of the angular dependence of the magnetization for $T>T_f$ of $(Y_{1-x}Gd_x)$-Mg-Zn have proved useful in the differentiation of effects due to crystal electric fields and those due to geometric demagnetization effects.

In what follows, we compare magnetic properties of Tb- and Gd-substituted icosahedral Y-Mg-Zn. The dc magnetization shows a similar behavior to the $(Y_{1-x}Tb_x)$-Mg-Zn data shown in Fig. 13, and the values of T_f obtained as described above are shown in the inset to Fig. 13. As for the Tb substitutions, T_f is lower for the smaller Gd concentration. However, perhaps surprisingly, the actual values of T_f for $(Y_{1-x}Gd_x)$-Mg-Zn are lower than those of $(Y_{1-x}Tb_x)$-Mg-Zn for similar x values, despite Gd^{3+} having the larger de Gennes factor $[(g-1)^2J(J+1)]$ of the two rare-earth ions. Hattori *et al.*[1] have reported a similar behavior for the pure Tb-Mg-Zn and Gd-Mg-Zn prepared by induction melting, and their data show T_f values (defined as the peak in the zfc dc magnetization) of 6.0 and 5.0 ± 0.5 K, respectively. As noted previously (Sec. II), Gd-Mg-Zn may be metastable, and we have been unable to grow single-grain samples from the ternary melt. These data may suggest that the $(Y_{1-x}Gd_x)$-Mg-Zn samples actually have a slightly different structure or composition to the other R-Mg-Zn samples, although this is thought to be unlikely. Of more interest is the possibility that these data may actually suggest that the lack of crystal electric-field effects for $R=$Gd can decrease T_f from that of $R=$Tb because the Gd^{3+} moments are isotropic. Some evidence to support this hypothesis comes from the Weiss temperatures of these different dilutions, and is discussed in detail below.

TABLE II. Summary of θ and T_f for the $(Y_{1-x}Tb_x)$-Mg-Zn series.

x	θ (K)	T_f[a] (K)
0.075	-2.1 ± 0.7	
0.15	-4.3 ± 0.2	
0.33	-9.2 ± 0.2	2.30 ± 0.05
0.50	-13.4 ± 0.2	3.40 ± 0.05
0.63	-16.9 ± 0.2	4.10 ± 0.05
0.75	-19.2 ± 0.2	4.80 ± 0.05
0.88	-22.7 ± 0.2	5.20 ± 0.05
1.00	-26.3 ± 0.2	5.80 ± 0.05

[a]Position of the maximum in zfc $\chi_{dc}(T)$.

Figure 14(a) shows the low-temperature part of the inverse dc susceptibility of the $(Y_{1-x}Tb_x)$-Mg-Zn samples, normalized by the experimentally determined Curie constant C for each concentration (obtained as described in Sec. IV A). Straight lines show the extrapolation of the high-temperature ($50<T<350$ K) fit of the Curie-Weiss law to the $\chi(T)$ data for each concentration x. The values of the Weiss temperatures obtained from the fits are given in Table II. Similar data and fits for $(Y_{1-x}Gd_x)$-Mg-Zn are shown in Fig. 14(b), and the corresponding Weiss temperatures are given in Table III. Note that for $x=0.075$ of both Tb and Gd

TABLE III. Summary of θ and T_f for the $(Y_{1-x}Gd_x)$-Mg-Zn series.

x	θ (K)	T_f (K)
0.075	-2.0 ± 0.9	
0.15	-5.8 ± 0.2	0.54 ± 0.05[a]
0.50	-21.0 ± 0.2	2.20 ± 0.05[b]
0.60	-23.6 ± 0.2	2.80 ± 0.05[b]

[a]Position of the maximum in zfc $\chi_{dc}(T)$.
[b]Position of the maximum in $\chi'_{ac}(T)$.

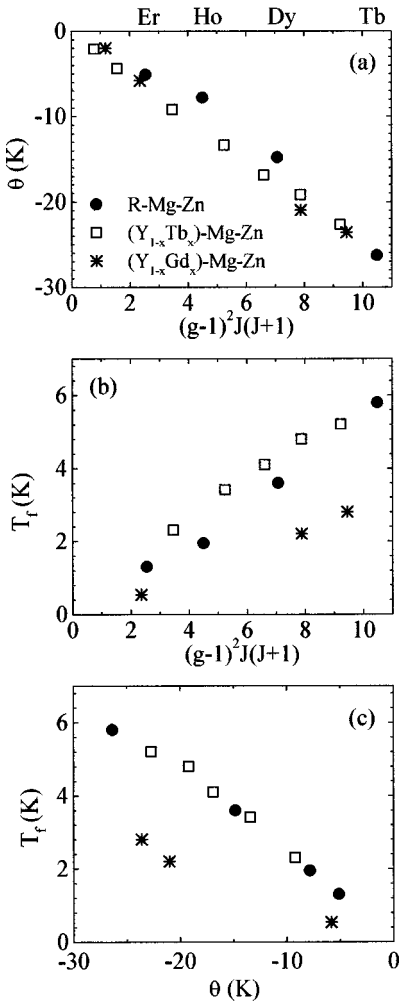

FIG. 15. The Weiss temperature (a) and the spin freezing temperature (b) vs the de Gennes factor for R-Mg-Zn (solid circles: R=Tb, Dy, Ho, and Er), $(Y_{1-x}Tb_x)$-Mg-Zn (open squares), and $(Y_{1-x}Gd_x)$-Mg-Zn (stars). Lower panel (c) shows the spin freezing temperature vs the de Gennes factor for the same compounds. Elemental symbols along the top of (a) indicate the de Gennes factor for the ternary R-Mg-Zn compounds. T_f values are from peak in zfc dc magnetization, except for Ho-Mg-Zn and Er-Mg-Zn, which are taken from ac susceptibility data shown in Fig. 10, and $(Y_{0.85}Gd_{0.15})$-Mg-Zn taken from ac susceptibility data in Table III.

dilutions, subtraction of the temperature-independent susceptibility due to Y-Mg-Zn (see Fig. 2) slightly alters the θ value obtained from Fig. 14, this difference being reflected in the slightly larger uncertainty in these two figures. This subtraction did not affect the larger magnetic rare-earth concentrations.

The inverse susceptibility data shown in Fig. 14 are particularly illuminating when considering the low-temperature deviation from the Curie-Weiss law as discussed previously with respect to the data in Fig. 3. We note that the deviations are smaller for smaller rare-earth concentrations, and are also present for the Gd dilutions. Neither of these effects would be expected if the deviations were due to CEF effects. These act on single ions, and hence should not show a concentration dependence, and also would not affect Gd^{3+} ions, for which the orbital angular momentum $L=0$. These data are therefore strong evidence that the deviation from Curie-

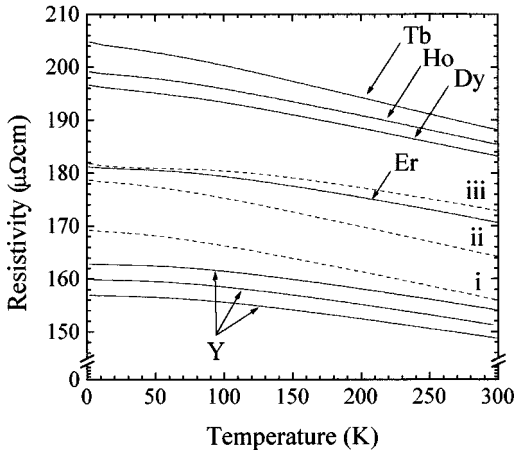

FIG. 16. Electrical resistivity as a function of temperature for icosahedral R-Mg-Zn (R=Y, Tb, Dy, Ho, and Er) and $(Y_{1-x}Tb_x)$-Mg-Zn for (i) $x=0.33$, (ii) $x=0.50$, and (iii) $x=0.88$. Note that there are three measurements of different Y-Mg-Zn samples. Note also the vertical axis break.

Weiss behavior a few Kelvin above T_f is indeed due to the preformation of antiferromagnetic clusters, as suggested in Sec. IV A.

As can be seen from Fig. 14, for similar magnetic rare-earth concentrations x, the Gd-containing samples have a larger Weiss temperature than the Tb-containing samples (e.g., for $x=0.50$, $\theta=-21.0$ K for the Gd substitutions, but $\theta=-13.4$ K for the Tb substitutions), consistent with de Gennes scaling of the antiferromagnetic interactions (see below). However, as described above, T_f is lower for the Gd-containing samples. To examine this more systematically, the de Gennes scaling of the Weiss temperatures of the R-Mg-Zn, $(Y_{1-x}Tb_x)$-Mg-Zn, and $(Y_{1-x}Gd_x)$-Mg-Zn samples is illustrated in Fig. 15(a). The data appear to fall onto a single line (with the mild exceptions of Ho-Mg-Zn and Dy-Mg-Zn that seem to have slightly smaller θ values than might be expected from the de Gennes scaling of the other compounds). Note in particular that the Tb and Gd dilutions follow the same de Gennes scaling. However, panel (b) of Fig. 15 illustrates the smaller T_f values for $(Y_{1-x}Gd_x)$-Mg-Zn than R-Mg-Zn or $(Y_{1-x}Tb_x)$-Mg-Zn compounds with similar de Gennes values. This is perhaps most clearly illustrated in Fig. 15(c) that shows the relationship between observed spin freezing temperatures and observed Weiss temperatures. The Weiss temperatures of the Gd dilution compounds de Gennes scale with the other compounds, reflecting that θ is a measure of the strength of exchange interaction. However, T_f appears to depend on more than just the strength of the exchange interaction, and for similar θ values the Gd dilution compounds have significantly lower T_f values than either R-Mg-Zn or $(Y_{1-x}Tb_x)$-Mg-Zn [Fig. 15(c)]. Note also, that despite the small deviations of Ho-Mg-Zn and Dy-Mg-Zn from de Gennes scaling of θ [Fig. 15(a)], these two compounds lie neatly on the single T_f vs θ line defined by R-Mg-Zn and $(Y_{1-x}Tb_x)$-Mg-Zn in Fig. 15(c).

Figure 15(c) clearly shows that for comparable coupling (as manifest by θ) the Gd series has T_f values a factor of 2 smaller than the other moment-bearing members. These data strongly suggest that the magnetic *isotropy* of the Gd local

moments leads to a lower T_f than might otherwise be expected from the de Gennes scaling of T_f of the other R-Mg-Zn compounds. This implies that both the aperiodicity of the R-R distances *and* the local CEF anisotropy contribute to the value of T_f. A similar behavior has also been observed for the spin-glass systems of Y and Sc doped with Tb and Gd.[20] More generally speaking, the non-CEF-split Gd moment is anticipated to lead to a Heisenberg spin glass, while the CEF-split Tb, Dy, Ho, and Er moments will be non-Heisenberg. Since the point symmetry of the rare-earth site(s) is as yet unknown, we do not know the nature of the anisotropy; i.e., we do not know if the sites are Ising, X-Y, or of some more complex nature. The factor-of-2 difference between the Heisenberg-like Gd series and the other moment-bearing rare earths is close to the factor of 3 seen between Heisenberg and Ising systems.[20]

G. Electrical resistivity

The electrical resistivity of the single-grain R-Mg-Zn samples (R=Y, Tb, Dy, Ho, and Er) is shown in Fig. 16 (note the vertical axis break). There is a good agreement between the measurements of the three different Y-Mg-Zn quasicrystals, giving confidence to the absolute value of $151 \pm 4\ \mu\Omega$ cm at 300 K. These values are a factor of almost 7 smaller than previous values obtained for polygrain Y-Mg-Zn samples,[23] likely due to the absence of grain-boundary scattering in our single-grain samples. The resistivity ρ is weakly temperature dependent, with a small negative $d\rho/dT$. Temperature dependence of this type is typical for icosahedral Al-Li-Cu (Ref. 24) and for a quasiperiodic direction of decagonal Al-Cu-Co (Ref. 25) and Al-Ni-Co.[26]

The magnetic rare-earth-bearing R-Mg-Zn quasicrystals (R=Tb, Dy, Ho, and Er) have higher resistivities than that of Y-Mg-Zn. As can be seen in Fig. 16, all follow a similar temperature dependence, with the Tb-, Ho-, and Dy-containing quasicrystals having room-temperature resistivity values of approximately 185 $\mu\Omega$ cm, Er-Mg-Zn having a value of 170 $\mu\Omega$ cm, whereas Y-Mg-Zn has a significantly lower value of 150 $\mu\Omega$ cm. These differences may be due to additional scattering from the rare-earth moments (although a difference of 40 $\mu\Omega$ cm between the resistivity of Y-Mg-Zn and Tb-Mg-Zn is difficult to reconcile with spin-disorder scattering), or to differences in the electronic structure of these compounds. There are no discernible features in the resistivity of the magnetic rare-earth-containing samples at the spin freezing temperature T_f, in agreement with the results of previous investigations probing $\rho(T)$ in spin glasses (see, for example, Refs. 27 and 28). Presumably, for $T<T_f$ the frozen-in randomness of the magnetic moments still significantly contributes to the resistivity.[12]

Also shown in Fig. 16 are the resistivities of three of the $(Y_{1-x}Tb_x)$-Mg-Zn samples (x=0.33, 0.50, and 0.88). The resistivity increases with Tb concentration x, although it is not clear how much of this increase is due to additional spin-disorder scattering from the Tb moments, how much is due to the additional static disorder arising from the rare-earth substitution, and how much is due to changes in the electronic structure. Note that the Tb substitution also appears to slightly affect the temperature dependence $d\rho/dT$ (Fig. 16).

V. DISCUSSION

Magnetization measurements of high-purity single-grain R-Mg-Zn samples (Fig. 3) show no evidence for long-range magnetic ordering of the rare-earth moments, even when considering $d(\chi T)/dT$ (Ref. 5) (proportional to the magnetic contribution to the specific-heat capacity close to an antiferromagnetic transition,[29] this is a particularly sensitive method to expose antiferromagnetic transitions). Furthermore, neutron-scattering experiments using crushed Tb-Mg-Zn single grains show no evidence for long-range magnetic ordering below 20 K.[5] However, weak peaks in neutron scattering results from rapidly cooled polygrain $Tb_8Mg_{42}Zn_{50}$ samples, with a propagation vector of $(\frac{1}{4},0,0,0,0,0)$, were reported in Ref. 4. This observation lead the authors to suggest that there is indeed a magnetic ordering of sorts above the spin-glass freezing temperature.[4] We note, however, that the R-Mg-Zn phase diagram is particularly rich, and other crystalline second phases may be responsible for the apparent long-range magnetic ordering observed in neutron-diffraction studies of polygrain samples. One possible candidate is discussed in the Appendix to this paper. As suggested in Ref. 5, it remains an open question as to whether the icosahedral R-Mg-Zn phase has a width of formation, and whether there is composition dependence to the long-range magnetic order claimed by Charrier, Ouladdiaf, and Schmitt.[4] Even so, long-range magnetic ordering in the R-Mg-Zn quasicrystals must be considered at best fragile, if not spurious. In addition, we note that deviations from Curie-Weiss behavior for temperatures just above the spin freezing transition are most probably associated with preformation of antiferromagnetic clusters, and is by no means evidence for long-range magnetic ordering.

There is, however, considerable evidence for a spin freezing transition in the magnetic rare earth containing R-Mg-Zn quasicrystals, with T_f between 1.35 and 5.8 K (see Table I). In particular, we note that the observation of a sharp negative anomaly in $\chi_3(T)$ (Fig. 9) for temperatures just above T_f is very compelling evidence to classify these materials as spin-glass systems. The spin-glass behavior arises from massive frustration of the magnetic interactions, this frustration probably having its origin in part in the multiplicity of R-R distances in the quasiperiodic environment. For all of the R-Mg-Zn quasicrystals studied (including the Tb and Gd dilutions in Y-Mg-Zn) Weiss temperatures (θ) scale with the de Gennes factor (Fig. 15), reflecting the fact that θ is a measure of the strength of the exchange interaction. However, the rare-earth concentration dependence of T_f for Tb and Gd dilutions in Y-Mg-Zn suggests that single-ion CEF effects have significant effects on the freezing temperature. Specifically, the non-CEF-split Gd (Heisenberg) system has significantly lower (by a factor of 2) freezing temperatures than the comparable CEF-split (non-Heisenberg) systems. Recent results of muon spin-rotation experiments show additional evidence for significant CEF effects in Tb-Mg-Zn.[30] It should be noted that the observation of an isotropic bulk magnetization for $T>T_f$ (Fig. 4) does not preclude these CEF effects, as the observed bulk magnetization is probably an average over many different rare-earth sites in the quasicrystal structure.

VI. CONCLUSIONS

Our detailed experimental investigation of the magnetic and electrical-transport properties of large, high-purity, well-ordered, self-flux grown, single-grain icosahedral quasicrystals in the R-Mg-Zn (R=Y, Tb, Dy, Ho, and Er) system leads to the following results. Based on the dc magnetization measurements, no evidence was found for a transition to a ground state with a long-range magnetic order in the temperature range between 2 and 300 K. For icosahedral R-Mg-Zn containing magnetic rare earths, the occurrence of an irreversible behavior of the dc magnetization and of a sharp cusp-type anomaly in the ac magnetic susceptibility at varying temperatures below 5.8 K indicate a spin freezing. Time-dependent relaxation of the dc magnetization below the freezing temperature T_f and a prominent negative anomaly in the third-order ac magnetic susceptibility near T_f reveal the spin-glass nature of this spin freezing. The electrical resistivity ρ is only weakly temperature dependent with a negative $d\rho/dT$. The absolute values of ρ fall in the range between 150 and 205 $\mu\Omega$ cm, indicating that the charge-carrier concentration must be fairly large compared to that of other thermodynamically stable icosahedral quasicrystals. The frequency dependence of the temperature at which maxima in the $\chi'_{\rm ac}(T)$ curves are centered and the T_f/x' ratios both lead to a classification of the icosahedral R-Mg-Zn containing magnetic rare earths as the RKKY spin glasses with a moderate interaction. Above T_f, the dc magnetization is isotropic within experimental resolution suggesting the existence of many different rare-earth sites. A comparative analysis of the magnetic properties of icosahedral $(Y_{1-x}Tb_x)$-Mg-Zn and $(Y_{1-x}Gd_x)$-Mg-Zn reveal that crystal-field effects significantly increase the freezing temperature T_f of the non-Heisenberg-like Tb series over the T_f values of the Heisenberg-like Gd series.

ACKNOWLEDGMENTS

We would like to thank A. I. Goldman, C. M. Soukoulis, and R. W. McCallum for many useful discussions, M. J. Kramer and Z. Islam for their structural work on the icosahedral and rhombohedral compounds, and M. J. Sailer for help in sample preparation. This work was in part supported by the Schweizerische National fonds zur Förderung der wissenschaftlichen Forschung. Ames Laboratory is operated for the U.S. Department of Energy under Contract No. W-7405-Eng-82. This work was supported by the Director for Energy Research, Office of Basic Energy Sciences.

APPENDIX: A CLOSELY RELATED CRYSTALLINE R-Mg-Zn PHASE

We note that the R-Mg-Zn ternary phase diagram is particularly rich. In Ref. 3, attention was drawn to a particular R-Mg-Zn crystalline phase that has a close composition to the icosahedral phase. This crystalline phase, which is not a periodic approximant of the icosahedral phase, might be a significant second phase in rapidly cooled growths. The structural and transport properties of this phase were reported in Ref. 3. Here we briefly discuss the magnetic properties.

Similarly to the quasicrystalline R-Mg-Zn phase, the crystalline R-Mg-Zn phase was also grown in single-crystal form from the ternary melt. Powder x-ray diffraction of crushed single crystals indicated that this phase is rhombohedral, with cell constants of a_R=16.95 Å and α=96.07° while electron microprobe analysis indicated a composition for the Tb-containing rhombohedral phase of approximately $Tb_7Mg_{31}Zn_{62}$ (quite close to the composition of the icosahedral phase: $Tb_9Mg_{34}Zn_{57}$).[3]

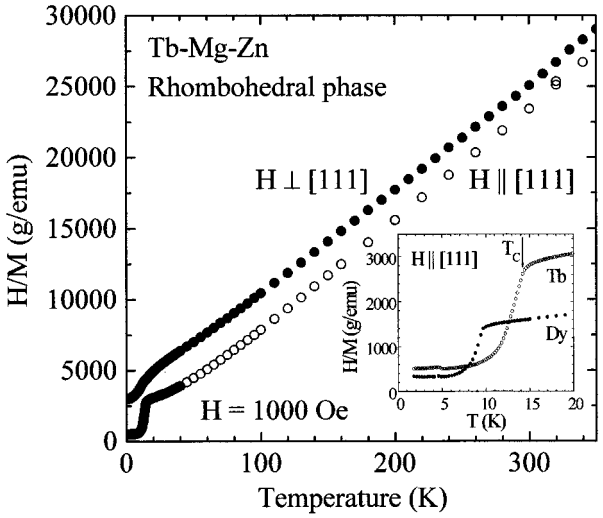

FIG. 17. The inverse magnetic susceptibility of the rhombohedral Tb-Mg-Zn phase, measured in an applied field of 1000 Oe applied both perpendicular (solid symbols) and parallel (open symbols) to the [111] rhombohedral direction. Inset shows low-temperature inverse magnetization for both Tb-Mg-Zn and Dy-Mg-Zn rhombohedral phases, with magnetic field applied parallel to [111]. Arrow indicates T_c for rhombohedral Tb-Mg-Zn estimated from resistivity $\rho(T)$ data (Ref. 3).

The dc magnetic susceptibility of the Tb-Mg-Zn rhombohedral phase measured in a magnetic field applied parallel and perpendicular to the [111] rhombohedral direction is shown in Fig. 17 as the plot of χ^{-1} vs T. The Curie constant based on the polycrystalline average obtained for $T>100$ K is consistent with the mass per Tb ion obtained via elemental analysis. The magnetization has an easy axis along the [111] rhombohedral direction, with a small, positive θ value, indicating predominantly ferromagnetic coupling between magnetic moments. The hard plane (perpendicular to [111]), on the other hand, has a small negative θ, indicating antiferromagnetic interactions. The inset to Fig. 17 shows the $\chi^{-1}(T)$ data on expanded scales for $H\|[111]$ (easy axis). Also shown in the inset are the $\chi^{-1}(T)$ data for rhombohedral Dy-Mg-Zn. Prominent features at approximately 14 and 9 K for Tb- and Dy-containing compounds, respectively, indicate a magnetic transition with some ferromagnetic component, however, $M(H)$ isotherms at low temperatures (not shown) indicate that the transition is not purely ferromagnetic. A phase transition at 14.2 K has previously been inferred from a sharp upturn in the zero-field electrical resistivity of rhombohedral Tb-Mg-Zn,[3] consistent with the magnetization data shown in the inset to Fig. 17. The temperature at which the upturn in the resistivity occurs is higher in larger applied fields.[3]

As evidenced by x-ray-diffraction studies,[5] nuclear peaks

from the *R*-Mg-Zn rhombohedral phase cannot account for all of the weak magnetic peaks reported for polygrain *R*-Mg-Zn quasicrystalline samples in Ref. 4. However, in low fields the magnetism does not appear to be a simple ferromagnetic ordering, and therefore may have a wave vector that is not commensurate with the nuclear order. The presence of this compound may explain some of the sharp magnetic peaks that Charrier, Ouladdiaf, and Schmitt[4] could not index, and the additional presence of other crystalline phases cannot be ruled out.

*Current address: Dept. of Applied Physics, Stanford University, Stanford, CA 94305.

[1] Y. Hattori, A. Niikura, A. P. Tsai, A. Inoue, T. Masumoto, K. Fukamichi, H. Aruga-Katori, and T. Goto, J. Phys.: Condens. Matter **7**, 2313 (1995).
[2] B. Charrier and D. Schmitt, J. Magn. Magn. Mater. **171**, 106 (1997).
[3] I. R. Fisher, Z. Islam, A. F. Panchula, K. O. Cheon, M. J. Kramer, P. C. Canfield, and A. I. Goldman, Philos. Mag. B **77**, 1601 (1998).
[4] B. Charrier, B. Ouladdiaf, and D. Schmitt, Phys. Rev. Lett. **78**, 4637 (1997).
[5] Z. Islam, I. R. Fisher, J. Zarestky, P. C. Canfield, C. Stassis, and A. I. Goldman, Phys. Rev. B **57**, 11 047 (1998).
[6] A. Langsdorf, F. Ritter, and W. Assmus, Philos. Mag. Lett. **75**, 381 (1997).
[7] A. P. Tsai, A. Niikura, A. Inoue, T. Masumoto, Y. Nishida, K. Tsuda, and M. Tanaka, Philos. Mag. Lett. **70**, 169 (1994).
[8] M. A. Chernikov, E. Felder, and H. R. Ott, Czech. J. Phys. **46**, Suppl. 4, 2161 (1996).
[9] A. F. J. Morgownik and J. A. Mydosh, Solid State Commun. **47**, 321 (1983).
[10] E. F. Wassermann, Physica B **109&110**, 1936 (1982).
[11] M. A. Chernikov, A. Bernasconi, C. Beeli, A. Schilling, and H. R. Ott, Phys. Rev. B **48**, 3058 (1993).
[12] J. A. Mydosh, in *Spin Glasses: An Experimental Introduction* (Taylor and Francis, London, 1993).
[13] R. V. Chamberlin, M. Hardiman, L. A. Turkevich, and R. Orbach, Phys. Rev. B **25**, 6720 (1982).
[14] J. R. L. de Almeida and D. J. Thouless, J. Phys. A **11**, 983 (1978).
[15] H. Sompolinsky, Phys. Rev. Lett. **47**, 935 (1981).
[16] A. P. Malozemoff, S. E. Barnes, and B. Barbara, Phys. Rev. Lett. **51**, 1704 (1983).
[17] K. Binder and A. P. Young, Rev. Mod. Phys. **58**, 801 (1986).
[18] J. L. Tholence, Solid State Commun. **35**, 113 (1980).
[19] J. L. Tholence and R. Tournier, J. Phys. (Paris), Colloq. **35**, C4-229 (1974).
[20] K. Baberschke, P. Pureur, A. Fert, R. Wendler, and S. Senoussi, Phys. Rev. B **29**, 4999 (1984).
[21] L. P. Lévy, Phys. Rev. B **38**, 4963 (1988).
[22] R. V. Chamberlin, G. Mozurkewich, and R. Orbach, Phys. Rev. Lett. **52**, 867 (1984).
[23] R. Kondo, Y. Honda, T. Hashimoto, K. Edagawa, and S. Takeuchi, in *Proceedings of the 5th International Conference on Quasicrystals*, edited by C. Janot and R. Mosseri (World Scientific, Singapore, 1995), p. 476.
[24] K. Kimura and S. Takeuchi, in *Quasicrystals: The State of the Art* (World Scientific, Singapore, 1991), p. 313.
[25] S. Lin, X. Wang, L. Lu, Z. Dian-Lin, L. X. He, and K. X. Kuo, Phys. Rev. B **41**, 9625 (1990).
[26] T. Shibuya, T. Hashimoto, and S. Takeuchi, J. Phys. Soc. Jpn. **59**, 1917 (1990).
[27] P. J. Ford and J. A. Mydosh, Phys. Rev. B **14**, 2057 (1976).
[28] M. A. Chernikov, A. Bernasconi, C. Beeli, and H. R. Ott, Europhys. Lett. **21**, 767 (1993).
[29] M. E. Fisher, Philos. Mag. **7**, 1731 (1962).
[30] D. R. Noakes, G. M. Kalvius, R. Wappling, C. E. Stronach, M. F. White, Jr., H. Saito, and K. Fukamichi, Phys. Lett. A **238**, 197 (1998).